Radar Antenna Scan Pattern Intelligent Recognition Using Visibility Graph

TAO WAN, XINYING FU, KAILI JIANG, YUAN ZHAO, AND BIN TANG

School of Information and Communication Engineering, University of Electronic Science and Technology of China, Chengdu 611731, China

Corresponding authors: Tao Wan (taowan.uestc0939@foxmail.com) and Kaili Jiang (jiangkelly@foxmail.com)

ABSTRACT Radar antenna scan pattern (RASP) reconnaissance is a major problem in electronic warfare (EW). The RASP exerts a considerable influence on target identification, jamming decision making, and electronic support measures and thus plays a critical role in modern electronic warfare. A visibility graph (VG) is a tool for converting a time series into complex graphs with excellent noise immunity. This paper proposes a novel method for the intelligent recognition of the RASP based on the VG, including the circular, sector, helical, raster, conical, phased array, phased array azimuth and circular elevation scans. The changes in the signal amplitude received from the EW receiver are determined. Moreover, the related features are extracted from the VG and utilized to classify the RASPs. The comparison experiments performed with different classifiers, such as machine learning, neural network, and deep learning, confirm that the proposed method can improve the robustness of the recognition rate to the noise and recognition accuracy.

INDEX TERMS Radar antenna scan pattern, visibility graph, feature extraction, deep learning, machine learning, neural network.

I. INTRODUCTION

The antenna scan type (AST) is a dominant parameter in the discrimination and solution of the ambiguities for the classification of radar threats. The antenna acts as a radiation device for radar electromagnetic energy, and its characteristics directly reflect the performance of the radar. To find the target, the radar antenna beam needs to search for the specified airspace in a certain manner, which corresponds to the scan of the antenna beam. The purpose and working state of radars are different, leading to different antenna beam shapes and antenna scan patterns (ASPs). The scan characteristics of an antenna can be used to locate the fixed pulse radar. More importantly, the accurate recognition of the ASP of the enemy radar is critical for the threat assessment. Furthermore, the ASP is key to identify the type and working state of the radar. Therefore, in modern electronic warfare, the recognition, in particular, the intelligent recognition of the radar ASP is an interesting yet challenging aspect. The research on the ASP can help in the analysis and identification of the threat target signals in complex electromagnetic environments in the future, thereby further strengthening the military. Such intelligent technology can improve the quality of work management

and realize full automation management, and it has a more reliable and comprehensive advantage over manual means.

As a part of radar reconnaissance, the scan pattern of traditional mechanical scan radars has been addressed in [3]–[8]; however, the counterpart for a phased array radar (PAR) has only begun to be explored. More specifically, a PAR has many advantages such as a fast scan beam, flexible beam shape, the ability of signal power synthesis in space, and easy formation of multiple beams [32]. Therefore, a PAR can achieve a low interception probability in the context of the beam pattern. However, this aspect is unfavorable for electronic reconnaissance. Therefore, accurately detecting and classifying the radar antenna scan pattern (RASP) is especially significant for future electronic warfare (EW).

In [3], the antenna scan pattern simulator (ASPS) was used to establish the signal graph of the time of arrival (TOA) versus that for the pulse amplitude (PA) for five scan patterns, including a circular scan, sector scan, helical scan, raster scan, and conical scan. Next, the authors extracted the signal features of the peaks, the number of main beams, amplitude variation of the main beams, and time differences between the main beams. Finally, the pattern classification of the RASP was performed using the naive Bayes (NB) algorithm, decision tree (DT), artificial neural network (ANN), and support vector machine (SVM). When the SNR was 20 dB,

The associate editor coordinating the review of this manuscript and approving it for publication was Sara Dadras.

the recognition probability was approximately 75%. In [4], the authors added the main beam flatness ratio as an extra feature. The recognition probability of the decision tree (DT), as a classification method to recognize seven scanning types, namely, conical, helical, spiral, circular, raster, sector, and electronic scans, has been considerably improved. Nevertheless, when the SNR is lower than 15 dB, the recognition probability decreases, and certain limitations pertaining to the PAR signal reconnaissance are encountered.

Moreover, a brief introduction of the radar signal model, including various scan patterns, was provided in [5], which reported on a mathematical model for the scan pattern and the parameters determining the power variation. The authors first determined the arrival time of the radar signal from the pulse repetition interval (PRI) of the RASP. Subsequently, they calculated the received signal strength and introduced several distortion factors. This approach exhibits a certain practicality; however, the model has limited types and thus cannot deal with the battlefield environment in real-time. A method to reduce the false identification was proposed in [7], in which the authors introduced a decision category based on the variance of the difference in the peak to peak intervals. The received signal amplitude was modeled for the RASP, and the position of the ES receiver and effect of the movement on the recognition accuracy were determined to analyze the trend of the misidentification. The average false identifications were approximately 82%, and the identification method for only the mechanical scan, and not the electronic scan, was considered.

Graph signal processing, which is widely used in image processing, pattern recognition, natural language processing, automatic control, and even electronic reconnaissance has been one of the most popular research topics in recent years. Among recent research [9], a method for converting a time series into a visibility graph (VG) was proposed. The algorithm maps a time series into a complex network. The main idea is to convert a time series into a complex network and perform the related processing on the network to feedback the information regarding the time series. In [10], a method of using the VG for bearing fault diagnosis was proposed. The authors extracted fifteen VG features from the VG matrix using network analysis and image processing methods. The authors identify the extracted features using the k-nearest neighbor (kNN), Lagrangian support vector machine (LSVM), and multilayer perception (MLP), and the accuracy of fault diagnosis was greater than 90%. In [11] , the VG was applied to the field of predictions. In the proposed method, the historical data were first converted into a VG matrix, and the link prediction strategy was subsequently used to predict future data. Finally, the future data were modified based on fuzzy logic. The results indicated that the use of fuzzy logic could improve the accuracy. The above research demonstrated that the use of the VG algorithm could improve the performance in the relevant field. Thus, we consider the introduction of the VG method in the field of radar reconnaissance.

To this end, this paper proposes a method combining the VG with machine learning, to be applied for RASP recognition. First, the mechanical scan and electronic scan equations are formulated. Second, the time series are converted into the contribution degree of the visibility graph. Subsequently, the feature extraction is performed by using the support vector machine, back propagation (BP) neural network, naive Bayes algorithm, MLP and deep belief network (DBN) [26]–[31]. The simulation results verify the feasibility of the proposed algorithm.

The novelty of this paper is that it presents, for the first time, a model expression for the various RASP types in a relatively complete manner. Moreover, we propose a method of combining the VG approach with machine learning and apply this combined technique for RASP recognition. Based on the idea of converting the time series into a complex network, we convert the modeling of the radar RASP into a VG network and perform the feature extraction of the generated network. The extracted features are recognized using classifiers. In summary, this paper aims to complement the effective recognition of the RASP in a complex electromagnetic environment to complement the reconnaissance of the RASP under low SNRs.

The remaining paper is structured as follows. Section II provides an overview of the VG and introduces the VG matrix representations for the scan patterns. Section III describes the RASP feature extraction based on the visibility graph. Section IV presents the validation of the proposed algorithm including the simulation experiment setup, results, and discussion. Section V concludes the paper and presents the potential future research directions.

II. SIGNAL MODEL

In this section, we first provide an overview of the proposed VG theory, present the four types of well-studied radar scanning patterns and derive the three radar scanning patterns that are rarely discussed in the electronic reconnaissance domain.

A. OVERVIEW OF VISIBILITY GRAPH

Assume that the coordinates for any three instants in a RASP are (t_α, A_α), (t_β, A_β), (t_γ, A_γ). If the visibility for points α and β is available, the points can be connected to the two nodes of the associated graph. If the point γ is between the two points, the following condition [9] is satisfied:

$$A_\gamma < A_\alpha + (A_\alpha - A_\beta)\frac{A_\beta - A_\gamma}{A_\beta - A_\alpha} \qquad (1)$$

To illustrate this aspect, a sample connection diagram for the conversion of the time series to a VG is shown in Fig. 1(a). The horizontal axis represents the time series, and the vertical axis represents the signal amplitude corresponding to the current time instant. l in the figure exhibits three properties, namely, connectivity (each node connects at least the nearest neighbors), undirected attributes (the VG is built without direction), and invariance under affine transformations (the connection properties remain unchanged when rescaling
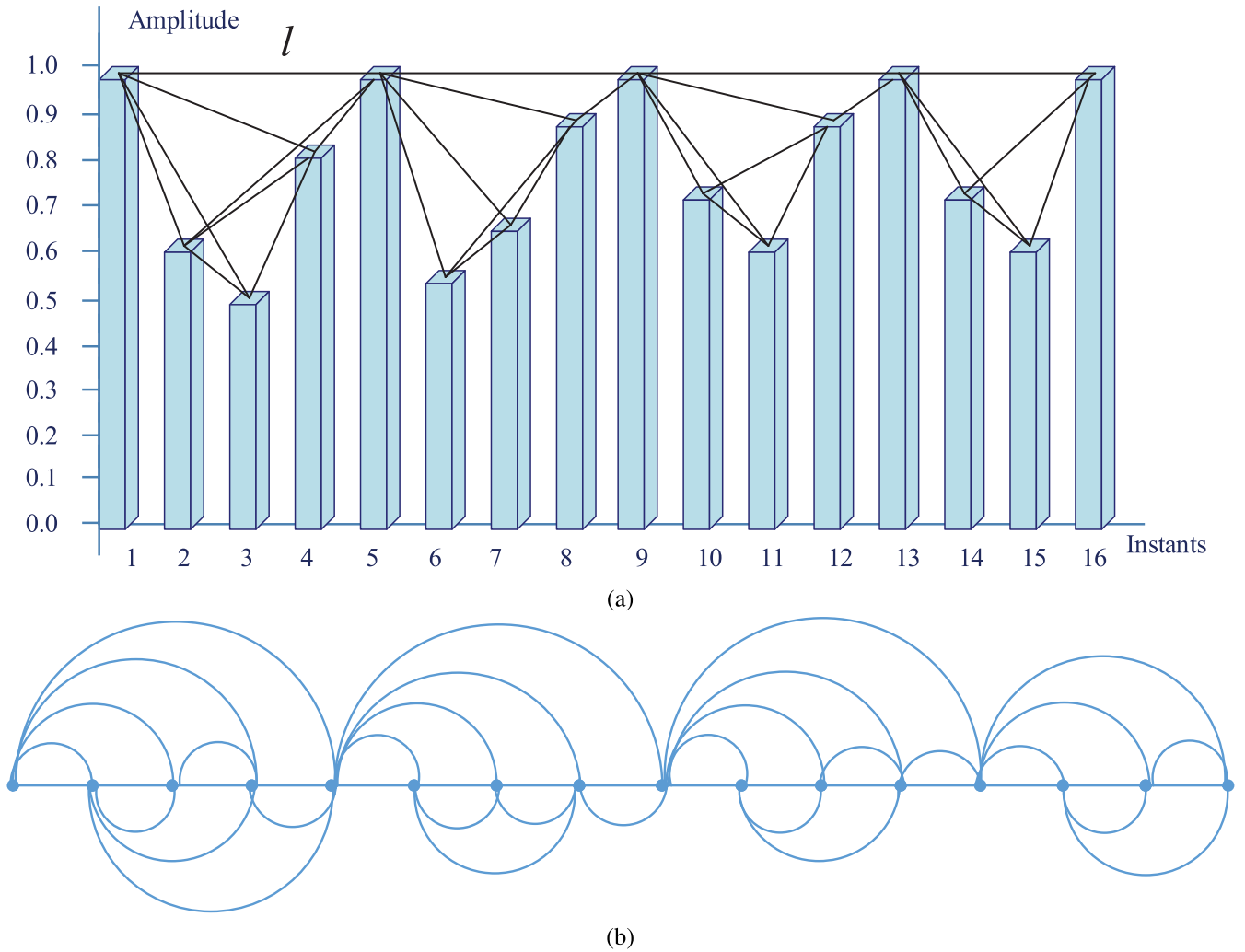
FIGURE 1. An illustration of N=16 instants versus signal amplitude between 0.5-1 for visibility graph algorithm. (a) Each node is connected to the line data; (b) A simplified diagram of the connection line corresponding points.

the horizontal and vertical coordinate axes or increasing or decreasing the signal amplitude).

The contour diagram corresponding to Fig. 1(a) is shown in Fig. 1(b) based on equation (1). Each time instant corresponds to a connection point, which can be directly connected with other points if a connection exists. In summary, there exists a straight line that connects the series data, provided that this 'visibility line' does not intersect any intermediate data heights [20].

The VG matrix of $N * N$ is defined as the degree distribution, which is the number of vertex connections in the visibility graph. Assuming that a connecting line exists between points α and β, the values of the αth column and βth row of the VG matrix are 1; otherwise, the values are 0. Following this rule, the VG matrix corresponding to Fig. 1 is constructed, as shown in Table 1. It can be noted that the degree distribution matrix has four distinct sets of data features corresponding to Fig. 1(b), and each set of data has no connection with that of other instants. These findings suggest

that the VG matrices are generally different for different time series.

TABLE 1. The degree distribution matrix of VG graph.

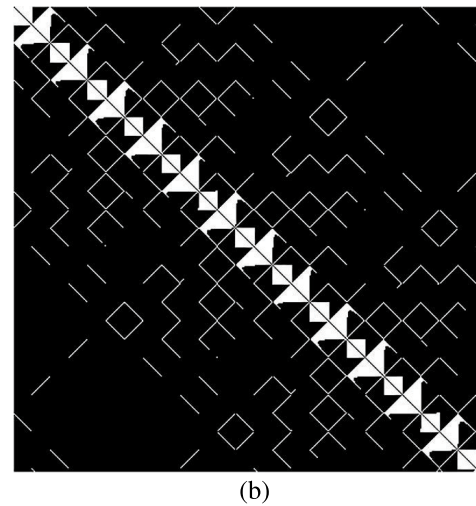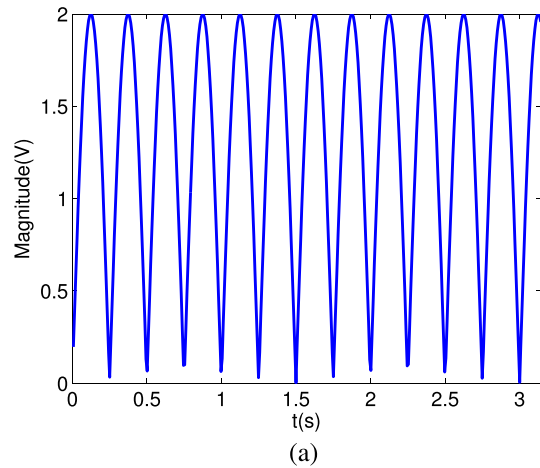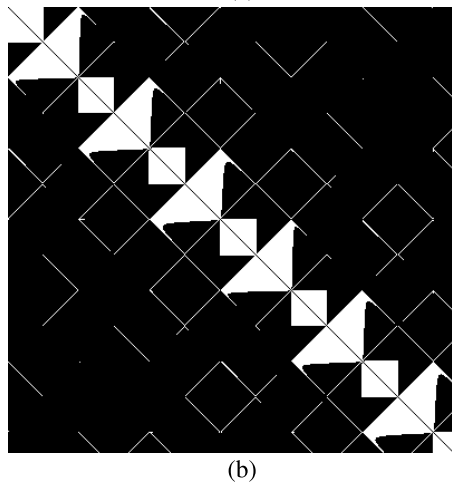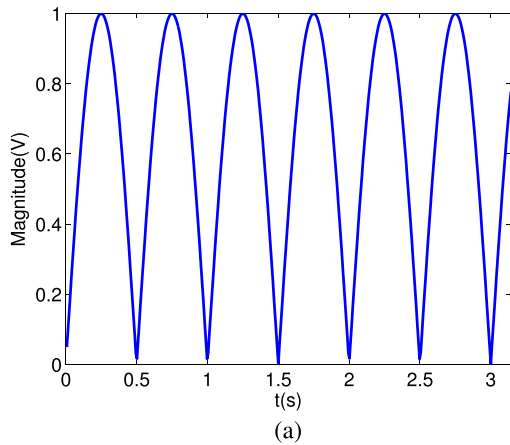| Instant	1	2	3	4	5	6	7	8	9	10	11	12	13	14	15	16
1	0	1	1	1	1	0	0	0	0	0	0	0	0	0	0	0
2	1	0	1	1	1	0	0	0	0	0	0	0	0	0	0	0
3	1	1	0	1	0	0	0	0	0	0	0	0	0	0	0	0
4	1	1	1	0	1	0	0	0	0	0	0	0	0	0	0	0
5	1	1	0	1	0	1	1	1	1	0	0	0	0	0	0	0
6	0	0	0	0	1	0	1	1	0	0	0	0	0	0	0	0
7	0	0	0	0	1	1	0	1	0	0	0	0	0	0	0	0
8	0	0	0	0	1	1	1	0	1	0	0	0	0	0	0	0
9	0	0	0	0	1	0	0	1	0	1	1	1	1	0	0	0
10	0	0	0	0	0	0	0	0	1	0	1	1	0	0	0	0
11	0	0	0	0	0	0	0	0	1	1	0	1	0	0	0	0
12	0	0	0	0	0	0	0	0	1	1	1	0	1	0	0	0
13	0	0	0	0	0	0	0	0	1	0	0	1	0	1	1	1
14	0	0	0	0	0	0	0	0	0	0	0	0	1	0	1	1
15	0	0	0	0	0	0	0	0	0	0	0	0	1	1	0	1
16	0	0	0	0	0	0	0	0	0	0	0	0	1	1	1	0

FIGURE 2. (a) Circular scan analysis diagram of PA versus time, (b)VG matrix converted by VG theory.

B. VG MATRIX REPRESENTATIONS FOR SCAN PATTERNS

Without loss of generality, we assume that the RASP can be varied, while the EW receiver is omnidirectional [34]. In addition, the signal observed by the EW receiver is contaminated by the additive random noise [13]–[15]. It was noted that for different RASPs, the VG matrix is also different, and thus the image corresponding to each RASP can be clearly distinguished.

1) CIRCULAR SCAN

In terms of electronic countermeasures, a circular scan is a classical RASP, which has azimuth and distance information but does not provide elevation information. The circular scan period may vary between 5 and 30 s [1], [4]. The amplitude of the pulse can be expressed as [6]

$$A_{pi} = A_p * F(\theta_i) * |\sin(\frac{\pi}{T_c}t)| * C_i \qquad (2)$$

where i represents the ith pulse, and the range of i is within a received signal pulse width; A_p is the signal amplitude; $F(\theta_i)$ is the horizontal beam gain as a function of the detected circular scan beam; T_c is the circular scan period; and C_i is the system amplitude stability coefficient of the intercepted circular scan pulse. Fig. 2(a) shows an analysis diagram

corresponding to the RASP in the circular scan pattern. Fig. 2(b) shows the VG matrix of the circular scan signal converted by the VG algorithm, which is represented as a two dimensional image.

2) SECTOR SCAN

A sector scan is similar to a circular scan, except that the sector scan pattern corresponds to a scan within only a certain angular interval. Such a scan pattern can increase the probability of intercepting short term signals [16]. The amplitude of the pulse can be expressed as [6]

$$A_{pi} = A_p * F(\theta_i) * [|\sin\frac{\pi}{T_{sf}}t| + |\sin\frac{\pi}{T_{sf}}(t - T_a)|] * C_i \quad (3)$$

where A_p is the signal amplitude, $F(\theta_i)$ is the horizontal beam gain function of the detected sector scan beam, T_{sf} is the sector scan period, T_a is the retrace interval of the fan sweep beam reaching the limit position and C_i is the system amplitude stability coefficient of the intercepted sector scan pulse. The sector scan analysis is shown in Fig. 3(a) when the intercepted receiver is in the middle of the scan angle interval. Fig. 3(b) is the VG matrix of the sector scan signal

FIGURE 3. (a) Sector scan analysis diagram of PA versus time, (b)VG matrix converted by VG theory.

converted using the VG algorithm, which is represented as a two dimensional image.

3) CONICAL SCAN

The conical scan pattern is generally used for target tracking [4], and the amplitude of the signal received is strongly related to the position of the EW receiver [2]. When the radar scans in a conical manner and the EW receiver is on the cone, the amplitude of the signal received is similar to that of the circular scan, which is a sinusoidal waveform with the largest amplitude. If the EW receiver is located within the cone except for at the center of the cone, the amplitude is also a sinusoidal waveform, and the signal amplitude is limited by the radius. If the EW receiver is located at the center of the cone, the distance from the radar to the EW receiver is fixed; therefore, the signal amplitude is fixed [3]. The amplitude of the pulse can be expressed as [6]

$$A_{pi} = A_0 * F(\theta_h) * |\sin(\frac{\pi}{T_{sb}} * t)| * C_h \qquad (4)$$

where $F(\theta_h)$ is the horizontal beam gain function value of the detected conical scan beam, T_{sb} is the conical scan period on the beam tilt axis, A_0 is the standard value of the pulse amplitude at the conical scan beam intercept point and C_h is the system amplitude stability factor of the intercepted cone scan pulse. It is interesting to observe that the conical scan pattern is basically similar to the circular scan pattern. Fig. 4(a) shows an analysis diagram corresponding to the RASP in the conical scan pattern. Fig. 4(b) shows the VG matrix of the conical scan signal converted using the VG algorithm, which is represented as a two dimensional image.

4) HELICAL SCAN

A helical scan is normally used in search states. The helical scan azimuth is omnidirectional, and the elevation angle is changed after each scan [18]. Therefore, the helical scan pattern includes not only the azimuth orientation information but also the elevation information. A higher scan frequency can be used during the helical scan to decrease the gap generated in the searching. When the detection distance for the EW receiver is R_r, the received power for the radar of interest can be expressed as [4]
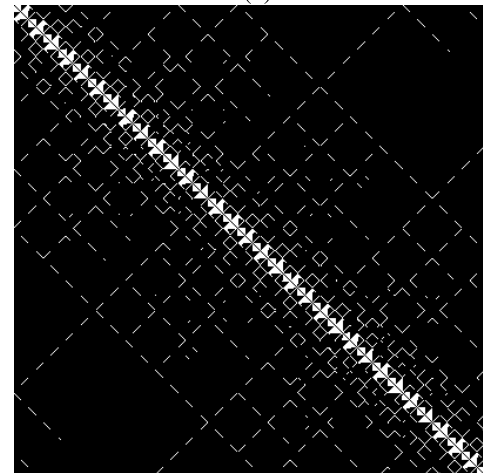
$$P_r = \frac{P_t G_{tr} G_r \lambda^2}{(4\pi)^2 R_r^2} \qquad (5)$$

where P_t is the radiated power from the radar of interest, G_{tr} is the gain of the transmission antenna in the direction of the reconnaissance receiver, G_r is the antenna gain of the EW receiver, and λ is the signal wavelength, respectively. When the EW receiver position and the radar position are determined, the four variables are the determined values, and the EW received power P_r is inversely proportional to R_r^2.

When the radar scans in the helical manner, R_r can be expressed as $\sqrt{(x'^2 + y'^2 + z'^2)}$. By Substituting the x', y', z' coordinates by $r\sin(\theta), r\cos(\theta), r\tan(\varphi)$, respectively,
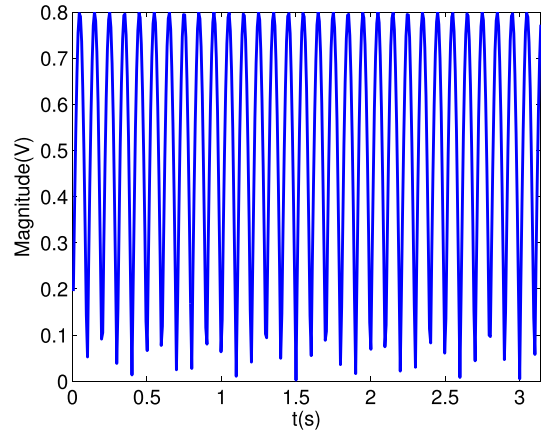
FIGURE 4. (a) Conical scan analysis diagram of PA versus time, (b)VG matrix converted by VG theory.

we can obtain

$$R_r^2 = 2r^2 - 2r^2 \cos(\theta) + r^2 \tan(\varphi) \qquad (6)$$

Further, the signal power received by the EW receiver can be rewritten as

$$P_r = \frac{P_t G_{tr} G_r \lambda^2}{(4\pi)^2 (2r^2 - 2r^2 \cos(\theta) + r^2 \tan(\varphi))} \qquad (7)$$

where θ is the angle between the radar beam and the Y axis, φ is the angle between the radar beam and the XOY plane, and r is the distance between the radar radiation source and the EW receiver. Subsequently, the problem can be transformed into the relationship between the angle of θ, φ and the helical scan period. Fig. 5(a) shows the helical scan analysis for the case in which the intercepted receiver is in the middle of the scan angle interval. Fig. 5(b) shows the VG matrix of the helical scan signal converted using the VG algorithm, which is represented as a two dimensional image.

5) RASTER SCAN

The raster scan pattern scans a sector using a set of parallel lines, and it is commonly used for the interception scan
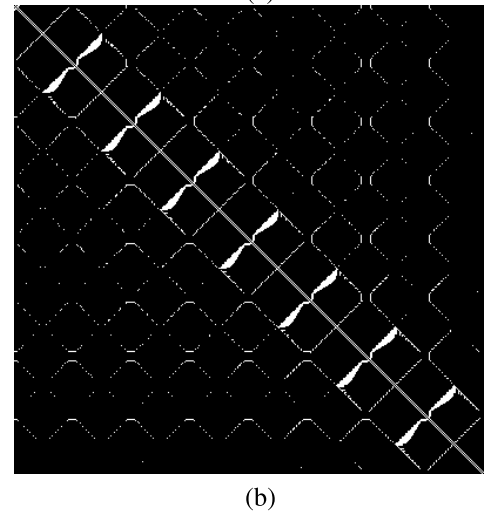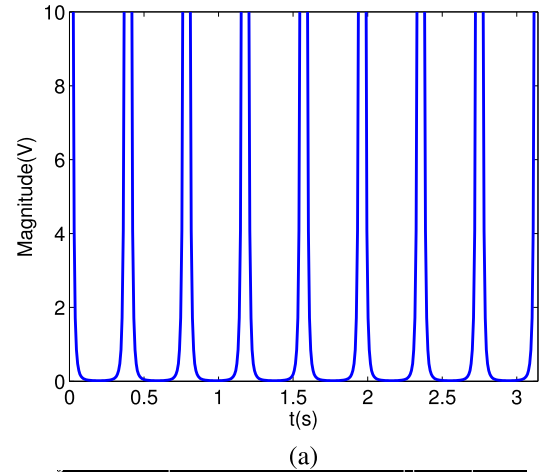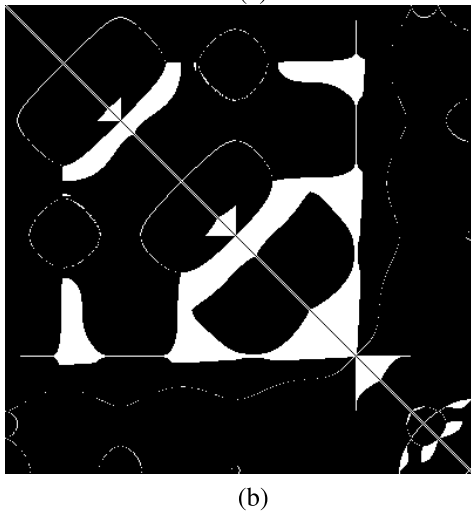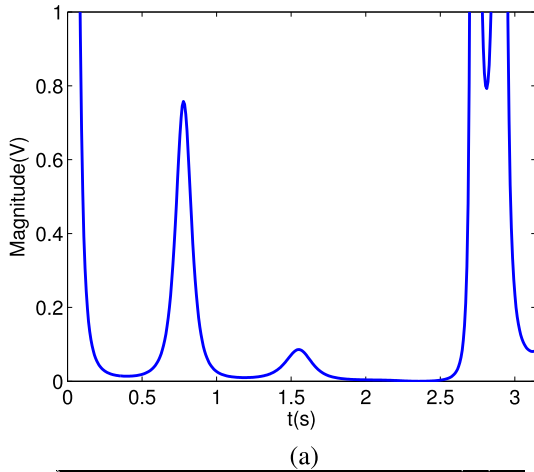
FIGURE 5. (a) Helical scan analysis diagram of PA versus time, (b)VG matrix converted by VG theory.

FIGURE 6. (a) Raster scan analysis diagram of PA versus time, (b)VG matrix converted by VG theory.

of airborne fire control radars. In a raster scan, the overlay volume is scanned line by line or column by column, and thus the raster scans also include azimuth and elevation information.

When the EW receiver receives the radar radiation source scan pattern as a raster scan, assuming that the azimuth angle between the EW receiver and the radar main beam is θ and the elevation angle is φ, the signal power detected is the same as that defined in equation (7). We assume that the grating azimuth angle is switched, that is, $W = 0$. In this paper, the attribute $\theta \in (0, 90°)$, $\varphi \in (0, 60°)$ is set. At this time, the changes in θ and φ can be written as

$$L = 2\pi r \frac{\theta}{360}$$

$$\begin{cases} \theta = \frac{vt}{r} * \frac{360°}{2\pi}, & \varphi = 0°, \; when 0 \le vt \le L \\ \theta = \frac{vt}{r} * \frac{360°}{2\pi} - 90°, & \varphi = 20°, \; when L < vt \le 2L \\ \theta = \frac{vt}{r} * \frac{360°}{2\pi} - 180°, & \varphi = 40°, \; when 2L < vt \le 3L \\ \theta = \frac{vt}{r} * \frac{360°}{2\pi} - 270°, & \varphi = 60°, \; when 3L < vt \le 4L \end{cases} \quad (8)$$

where v is the raster scan rate, L is the length of the raster scan column, and r is the distance between the radar beam and the EW receiver. The raster scan pattern analysis is shown in Fig. 6(a), and Fig. 6(b) shows the VG matrix of the helical scan signal converted using VG algorithm, which is represented as a two dimensional image.

6) PHASED ARRAY SCAN
The advantage of a phased array radar (PAR) is that the PA is a constant and not a function of time, as in the case of a mechanical scan radar. However, the PAR scan pattern is generally electronically scanned, and it can be randomly changed from one direction to the other via phase control. In this case, the EW receiver cannot obtain the PA versus time information. The PARs can realize time tracking and searching (TAS) in a specific area, and the target searching is performed according to the regularity. A target is illuminated for a limited time interval that is periodically repeated according to the number of targets. The illumination time interval is determined by the beam dwell time of the electronic scan, which occupies one or more coherent processing intervals of the PAR. The PAR shown in Fig. 7(a) corresponds to the
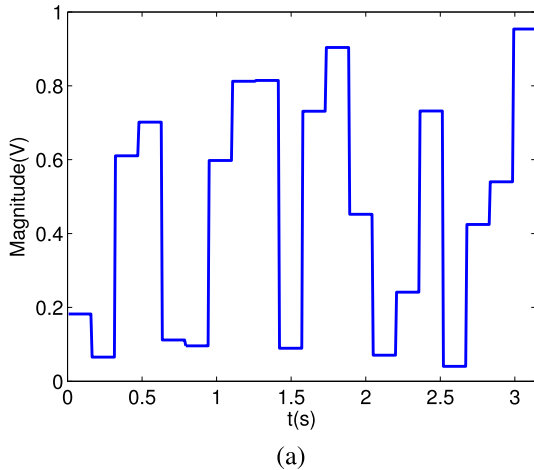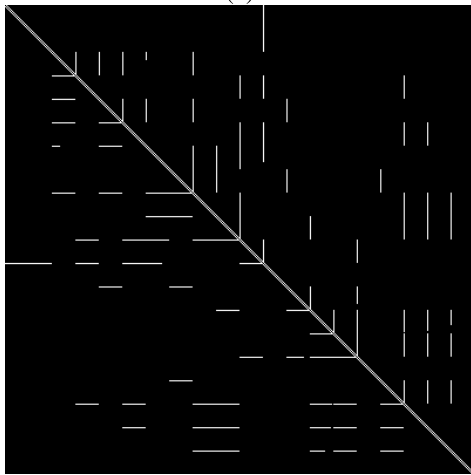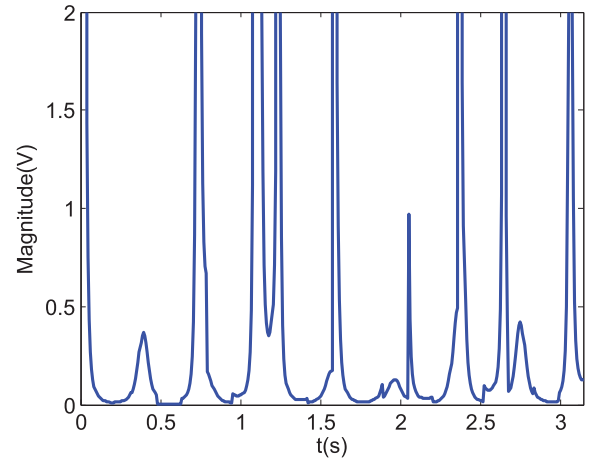
FIGURE 7. (a)Phased array radar scan analysis diagram of PA versus time, (b)VG matrix converted by VG theory.

FIGURE 8. (a)Phased array azimuth scan and circular elevation scan analysis diagram of PA versus time, (b)VG matrix converted by VG theory.

case when the intercepted receiver is in the middle of the scan angle interval. Fig. 7(b) shows the VG matrix of the PAR signal converted using the VG algorithm, which is represented as a two dimensional image.
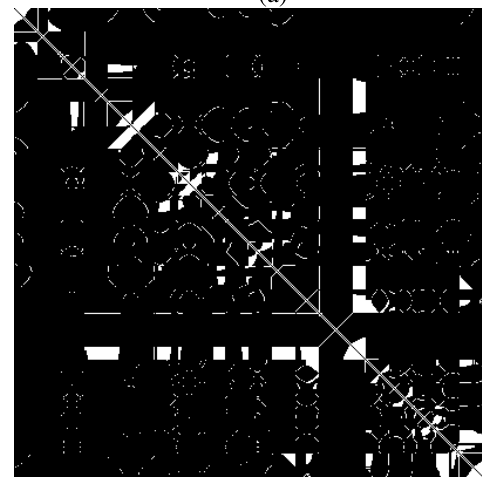
7) PHASED ARRAY AZIMUTH SCAN AND CIRCULAR ELEVATION SCAN

The PAR consisting of a line array only has a 2D scan, and the 3D scanning needs to expand the array. However, as a compromise, the PAR azimuth scan and circular elevation scan can be used to implement a three coordinate search. The combination of the phased array azimuth scan and circular elevation scan is generally used for a target search, tracking and measurement mission. In this paper, we assume that the circular scan of the azimuth is a threat antenna, and the phased array of the elevation angle can control the angle arbitrarily. In this case, the beam irradiation time can be obtained by the beam dwell time, although the beam amplitude is still random.

From the EW side, the scan pattern in the azimuth direction is a circular scan, and it can be recognized by observing

the number of pulses, repetition scan period and possible number of discrete beam positions. Since the coordinates of R_r in the stereo coordinate system are the same as those of the previous scan, as shown in Fig. 8, the signal power of the EW receiver is the same as that obtained using equation (7). Fig. 8(b) is the VG matrix of the phased array azimuth scan and circular elevation scan signal converted using the VG algorithm, which is represented as a two dimensional image. Nevertheless, the elevation angle φ changes randomly at this time, and the azimuth θ changes uniformly.

The above discussion indicates that there exists a strong correlation between the various scanning methods, and it is difficult to distinguish them from each other. In addition, we found that for the RASP, the influencing factors include mainly two aspects: 1: the length of the time series, i.e., the number of signal points, and 2: the noise, that is, a larger signal noise corresponds to a larger recognition error. The VG can transform the time series into a complex network. The existing literature indicates that it is considerably easier to extract the network features and later identify them.

III. RASP FEATURE EXTRACTION BASED ON VISIBILITY GRAPH

A. FEATURES OF VISIBILITY GRAPH

The relevant theory of the VG has been introduced in the previous section. The VG has been applied in various fields [10]–[13]. The signal of the EW receiver received from the RASP exhibits a time series distribution, and thus the VG method can be applied to the RASP research. This section introduces several types of features of the related VG algorithms [19].

1) AVERAGE DEGREE

Table 1 indicated that different RASPs have different degree distribution matrices. The average degree is the most intuitive feature that reflects the complexity of a VG map, and it can be expressed as

$$\overline{d} = \frac{1}{N} \sum_{i=1}^{N} d_i \qquad (9)$$

The concept of the average degree reflects the connection of each node of the time series. It is known from the graph theory that the average degree is proportional to the stability of the system.

2) AVERAGE CLUSTERING COEFFICIENT

The concept of the average clustering coefficients was first proposed in [21]. The definition of average clustering coefficients can be expressed as

$$C_i = \frac{(A^3)_{ii}}{(A^2)_{ii}[(A^2)_{ii} - 1]}, \quad \overline{C} = \frac{1}{N} \sum_{i=1}^{N} C_i \qquad (10)$$

In the RASP, the average clustering coefficient reflects the clustering of the VG matrix. Equation (15) shows that $\overline{C}$ is in the $0-1$ interval, and the clustering situation is positively correlated with the size of $\overline{C}$. Therefore, we choose the average clustering coefficient as the second feature.

3) NEWMAN COORDINATION COEFFICIENT

Literature [22] proposes a hybrid network model, which is defined as a network in which a cooperative mix of the nodes with many connections in the network tends to connect to other nodes with many connections. In the context of the RASP, this aspect reflects the penetration and robustness of the different scan patterns. In the simplest case, a network is represented by an undirected graph of N vertices and M, which can be represented as

$$r = \frac{M^{-1} \sum\limits_{e_{ij} \in \varepsilon} d_i d_j - \left[M^{-1} \sum\limits_{e_{ij} \in \varepsilon} \frac{1}{2}(d_i + d_j) \right]^2}{M^{-1} \sum\limits_{e_{ij} \in \varepsilon} \frac{1}{2}(d_i^2 + d_j^2) - \left[M^{-1} \sum\limits_{e_{ij} \in \varepsilon} \frac{1}{2}(d_i + d_j) \right]^{2'}} \qquad (11)$$

where d_i, d_j are the degrees of the vertices at the ends of the ith edge, with $i = 1; \ldots; M$. Obviously, the range of r is -1 to 1.

When $r \leq 0$, it is completely uncoordinated. When $r > 0$, the network is fully coordinated. The fully coordinated networks are more easily penetrated, and they are more robust to the removal of their highest vertices. The uncoordinated networks are less penetrated and more vulnerable to attacks. Therefore, we use the Newman coordination coefficient as the third feature.

4) NORMALIZED NETWORK STRUCTURE ENTROPY

From the information theory [23], we know that

$$E = - \sum_i I_i * \ln I_i \qquad (12)$$

This aspect is known as the network structure entropy [24]. Here, I_i represents the probability of the occurrence of event i, where i ranges from 1 to the VG network maximum. When the network connection has N connection points, the network complexity is the highest. In this case, nts in the network structure are N, the network complexity is the largest. Then $E_{\max} = - \sum_i \frac{1}{N} * \ln \frac{1}{N} = \ln N$. When all the connection points in the network structure are only connected to a certain point in the middle, we assume that all the nodes are connected to the first node, that is, $k_1 = N - 1, k_j = 1(j \neq 1)$. In this case, the network is the most uneven, and the network structure entropy is the smallest. When $I_1 = \frac{1}{2}, I_j = \frac{1}{2(N-1)}(j \neq 1)$, and $j = 1$, a network, cannot be formulated. Therefore, by considering $j = 2$, we can obtain the following expression:

$$E_{\min} = - \sum_{j=2}^{N} I_j * \ln I_j = - \sum_{j=2}^{N} \frac{1}{2(N-1)} * \ln \frac{1}{2(N-1)}$$
$$= -(N-1)\frac{1}{2(N-1)} \ln \frac{1}{2(N-1)} = \frac{\ln 2(N-1)}{2} \qquad (13)$$

To eliminate the influence of the number of vertices on the entropy of the network structure, we introduce the concept of the normalized network structure entropy, which can be written as

$$E_{norm} = \frac{E - E_{\min}}{E_{\max} - E_{\min}} = \frac{-2 \sum\limits_{i=1}^{N} I_i * \ln I_i - \ln 2(N-1)}{2 \ln N - \ln 2(N-1)} \qquad (14)$$

We use the normalized network structure entropy as the fourth feature.

5) VG COMPLEXITY

The eigenvalues of all the neighbor matrices of the VG graph are real numbers, and the largest one is recorded as $r_{\max}$. Hence, $2 \cos(\pi/(N + 1)) \leq r_{\max} \leq N - 1$, and the VG complexity can be defined as [24]

$$C_r = 4c_r(1 - c_r), c_r = \frac{r_{\max} - 2 \cos \frac{\pi}{N+1}}{N - 1 - 2 \cos \frac{\pi}{N+1}} \qquad (15)$$

C_r satisfies the inequality $0 \leq C_r \leq 1$, and it has been proved that the VG complexity depends largely on the number

of edges. The use of the VG complexity has been used to distinguish between electroencephalograms (EEGs) [25] and perform error diagnoses [10]. Therefore, this paper uses the VG complexity as the fifth feature to study the RASP.

6) VG DENSITY

The VG density can directly reflect the size of the graph, and the VG density can be represented by a VG neighbor matrix. This density can be expressed as [10]

$$G_d = \frac{\sum_{i,j} m_{i,j}}{N(N-1)} \quad (16)$$

where G denotes the VG obtained from the signal received from the EW receiver, and the range of values of i and j is from 1 to the maximum value of the VG network. As for RASP, the density G_d of G is defined as the ratio of the number of edges in the graph to the number of possible edges, and d represents the neighboring matrix of the visibility graph. This paper selects the VG density as the sixth feature.

B. CLASSIFIER

The sensitivity of the EW receiver is higher than that of the radar warning receiver (RWR). Nevertheless, the signal range of interest is different for different RASPs, and thus the EW receiver may need to process many parameters. For the LPI radar signal, the intercepted signal has a low SNR and features low sidelobes and frequency hopping [33]. Therefore, the study reported in this paper is similar to that in the previous article [3], [4], assuming that the EW receiver receives the radar main lobe and assumes that the required preprocessing has been completed. The six features introduced in the previous section are used for the classification training involving the BP neural network, NB, SVM, MLP, and DBN.

1) BP NEURAL NETWORK

The BP neural network [26] is a multilayer feedforward network trained through error back propagation. The corresponding algorithm is called the BP algorithm, and the main concept is that of the gradient descent method. The gradient search technology is used to finally fulfill the actual output value of the network. The mean square error of the expected output value is minimal.

2) NB

The NB algorithm [27] assumes that the features are independent of each other. This assumption makes the naive Bayesian algorithm simple but sometimes sacrifices certain classification accuracy. The NB criterion algorithm flow as shown in Algorithm 1.

3) SVM

The purpose of the SVM [28] is to find a hyperplane to segment the sample. The principle of segmentation is to maximize the interval and finally transform it into a convex

---

Algorithm 1 Overview of NB Algorithm

Require:

Set the training set is j samples, n dimensions $T = (x_1, y_1), (x_2, y_2), \ldots, (x_j, y_j)$, k is feature output categories, $y \in \{c_1, c_2, \ldots, c_k\}$, respectively

Ensure:

Instance $X_{(test)}$

1: Calculate the K prior probabilities of Y: $P(Y = c_k)$
2: Calculate the conditional probability distribution
   $P(X = x|Y = c_k) = \prod_{j=1}^{n} P(X^{(j)} = x^{(j)}|Y = c_k)$
3: Calculate the posterior probability according to the Bayesian principle
   $P(Y = c_k|X = x) = \frac{P(X=x|Y=c_k)P(Y=c_k)}{\sum_k P(X=x|Y=c_k)P(Y=c_k)}$
4: Bring in
   $P(X = x|Y = c_k) = \prod_{j=1}^{n} P(X^{(j)} = x^{(j)}|Y = c_k)$,
   the above formula can be converted to
   $P(Y = c_k|X = x)$
   $= \prod_{j=1}^{n} P(X^{(j)} = x^{(j)}|Y = c_k) P(Y = c_k)$
5: **return** Calculate $X_{(test)}$ category $y_{(test)} =$
   $\arg\max_{c_k} \prod_{j=1}^{n} P(X^{(j)} = x^{(j)}_{(test)}|Y = c_k) P(Y = c_k)$

---

quadratic programming problem. The SVM includes the following models. When the training samples are linearly separable, a linear separable support vector machine is learned by maximizing the hard interval. When the training samples are approximately linearly separable, a linear support vector is learned by maximizing the soft interval. When the training samples are linearly inseparable, a nonlinear support vector machine is learned by using the kernel techniques and soft interval maximization.

4) MLP

The MLP is a forward structured artificial neural network that maps a set of input vectors to a set of output vectors. The MLP can be thought of as a directed graph consisting of multiple node layers, with each layer connected to the next layer. In addition to the input nodes, each node is a neuron (or processing unit) with a nonlinear activation function. A supervised learning method called the backpropagation algorithm is normally used to train the MLP. The MLP is a generalization of perceptrons; consequently, this approach overcomes the limitation of the perceptrons being unable to achieve linear indivisible data recognition.

5) DBN

The deep belief network is proposed to simplify the logistic trusted network [31]. This network can model the data probability distribution or directly classify the data. The DBN consists of undirected and directed parts. As shown in Fig. 9, the upper part is an undirected graph, which constitutes an associative memory network and is also a restricted Boltzmann machine. The remaining part is a directed graph. The top-down recognition weight is only used to infer, and it does not form a part of the model.
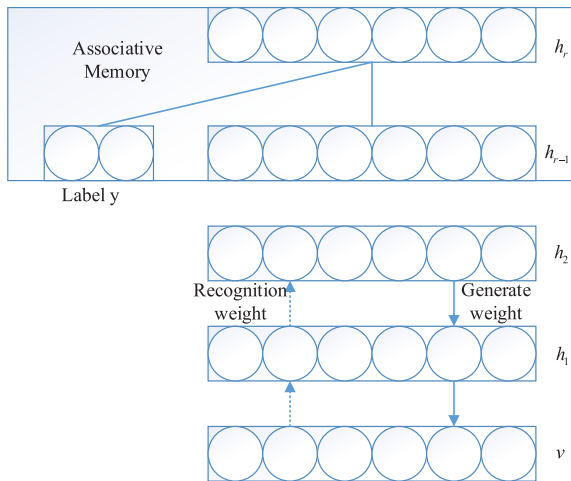
FIGURE 9. Deep belief network structure.

In Fig. 9, we can see the visible vector v and the implicit vector $h_k = (h_{k,1}, h_{k,2}, \ldots, h_{k,n})$, $k = 1, 2, \ldots, r$ from the bottom to top. The generated weight between the visible layer and the first hidden layer is represented by G^1, and the identification weight is represented by W^1. The weights for the other layers are represented in a similar manner. y represents the label vector, and the label layer and the rth hidden layer are also undirected connections. Thus, the joint probability distribution of the DBN can be expressed as [31]

$$p(v, y, h_1, h_2, \ldots, h_r | \theta) \oplus$$
$$= p(v|h)p(h_1|h_2) \cdots p(h_{r-2}|h_{r-1})p((y, h_{r-1}), h_r) \quad (17)$$

where θ is the parameter set, $p((y, h_{r-1}), h_r)$ is treated as a visible vector with (y, h_{r-1}), and we consider a constrained Boltzmann machine with h_r as the implied vector. The DBN learning process can be divided into two phases. The first phase is the unsupervised pretraining of the restricted Boltzmann machine, and the second phase is tuned using the wake-sleep algorithm. The unsupervised training phase mainly estimates the conditional probability corresponding to the restricted Boltzmann machine, and it later estimates the conditional probability of each layer of the DBN. The wake-up algorithm is divided into two parts: waking up and sleeping. The waking up part is a bottom-up process, whose aim is to repeatedly use the recognition weight and the recognition offset to estimate the generated weight and the generated offset. This process is in contrast to that involving the constant iteration of updating the weights and offsets.

IV. EXPERIMENTAL RESULTS

The section describes the performance of the VG algorithm for the RASP. The properties of the VG algorithm are analyzed using a set of Monte Carlo simulations, and the VG algorithm is combined with the classification algorithms for different SNRs. The experimental results suggest that this method exhibits not only a satisfactory classification performance but also excellent robustness to noise.

Algorithm 2 Overview of RASP Recognition Algorithm

Require:
  EW receiver detects radar signal amplitude signal
  Set EW receiver model parameters and detection parameters
Ensure:
 1: Construct the visibility graph model
 2: Send the EW receiver detection model to the visibility graph and build the complex network
 3: Feature extraction of the constructed complex network
 4: Classification and identification of features by each classifier
 5: **return** model parameters and detection parameters

A. SIMULATION EXPERIMENT SETUP

We recall that the EW receiver observes the signal amplitude, knows the time series, and constructs the matrix VG degree distribution. This subsection provides a detailed description of the implementation and evaluation process of the proposed RASP recognition algorithm. We briefly introduce the experimental setup, performance metrics and employed datasets.

1) PERFORMANCE METRICS

The experiments were conducted on a Windows system. All the experiments were run on the same machine with an Intel(R) Core (TM) i7, CPU 3.60 GHz, and 16 GB RAM. The implementation of the proposed approach encompasses the SVM, BP neural network, NB, MLP, and DBN, which were realized using a simulation experiment. The simulation parameters used in this paper are listed in Table 2.

In this paper, we use the following suite of statistical metrics for the performance evaluation of the RASP recognition:

1) Successful recognition probability (SRP): This metric defines the proportion of the recognition cases that were correctly predicted relative to the predicted size of the RASP class. The metric can be expressed as $SRP = \frac{TR}{TR+FR}$, where TR and FR denote true and false recognitions, respectively.

2) Computational time (CT): This metric describes how long a particular algorithm spends on the model for a complete dataset.

2) DATASET

In this subsection, we introduce the RASP used in the proposed classifier. Although the RASP in the proposed recognition technology is based on the RASP400 (i.e., the RASP with input images sized $400 * 400$ pixels), certain modifications are made to the RASP400 to make it fit the proposed RASP. Taking DBN as an example, the first modification is that the data of the original training set are converted from $400 * 400 * 7$ to $3360 * 5$, and then, the data of the test set are converted to $672 * 5$, ensuring that the test set is 20% of the training set. Simultaneously, to speed up the classification while maintaining accuracy, we attempt to reduce the number of network parameters.

TABLE 2. Simulation parameters for the intercepted radar signal.

Parameter settings	Units	Magnitude
The horizontal beam gain function value of the intercepted scanning beam	$F(\theta_i)$	1
Scanning period	T_s	4ns
The amplitude stability coefficient of the system of intercepting the scanning pulse	C_i	1
The retrace interval of the sector scanning beam reaching the limit position	T_a	0.5ns
Radiation source transmission power	P_t	1dB
Gain of the transmitting antenna in the direction of the reconnaissance receiver	G_{tr}	1
Signal wavelength	λ	$5 * 10^{-6}$
Azimuth in different scanning modes	θ	$(0, 2pi)$
Antenna gain	G_r	1
PAR beam dwell time	t	0.1s
Interval of elevation angle	β_s	$(20°, 60°)$
Elevation in different scanning modes	ϕ	$(0, 60°)$
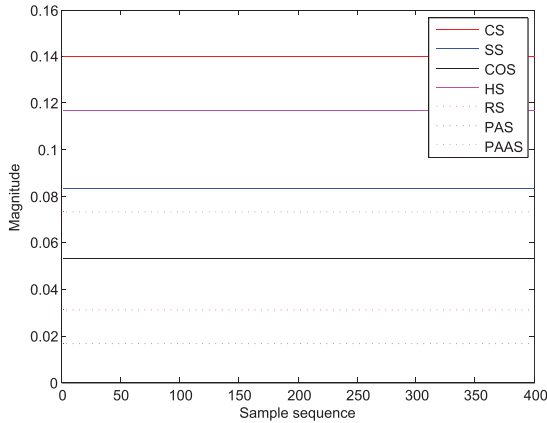
(a)
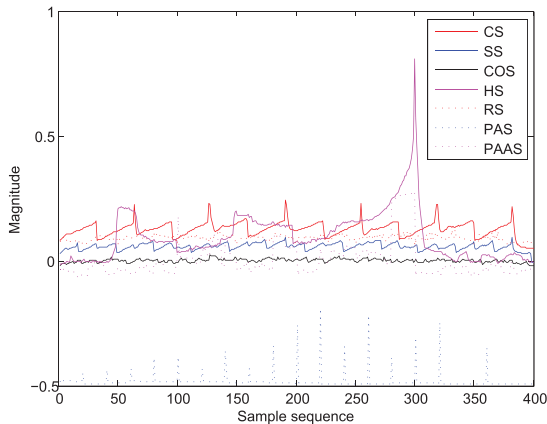
(b)

FIGURE 10. Related features of RASP on visibility graphs. (a)VGD, (b) ACC.

After the received RASP signal is converted to the visibility graphs, the (1) average degree; (2) average clustering coefficient (ACC); (3) Newman coordination coefficient; (4) normalized network structure entropy (5) visibility graph complexity, and (6) visibility graph density (VGD) are selected to perform the RASP recognition. The circular scan (CS), sector scan (SS), conical scan (COS), helical scan (HS), raster scan (RS), phased array scan (PAS), phased array azimuth scan and circular elevation scan (PAAS) are performed for the feature extraction. The ACC and VGD are taken as examples to depict the various RASPs after feature extraction, as shown in Fig. 10. In the figure,
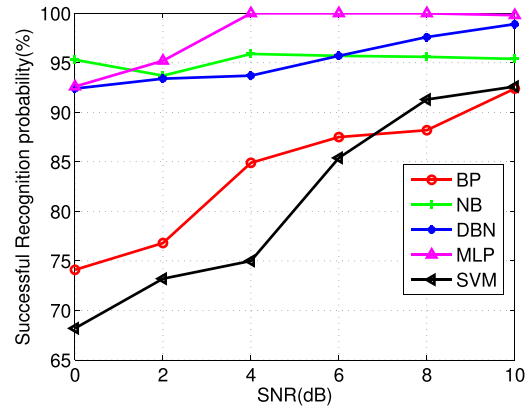

FIGURE 11. Performance of each classifier under different SNR.

we can see that the different RASPs have a large degree of discrimination, and the other features are similar. The VGD can be noted to be the most notable of the six feature extraction algorithms, and the ACC is the most confusing, although it still exhibits a clear distinction. Therefore, we can conclude that the VG after feature extraction can distinguish each kind of RASP.

B. EXPERIMENTAL RESULTS AND DISCUSSION

This subsection presents a comparison of the implemented approach and the state of the art methods. According to the VG features described in Chapter 4, a classifier was used to classify and identify the VG features. The features were classified in the experiment using the five classifiers described above. We compared the performance of the proposed VG algorithm with the recent algorithms [3], [7] and performed several Monte Carlo simulation experiments.

The first experiment involved the direct comparison of each classifier, namely, the SVM, BP neural network, NB, MLP, DBN, which were classified by the features that can be extracted by the visibility graph. In this experiment, we varied the SNR from 0-10 dB, and the performance of each classifier is as shown in Fig. 11.

Fig. 11 shows that the performance of the MLP and DBN classifiers is better than that of the SVM and BP neural network. The performance of the NB exhibits a high steady state. The average successful recognition probabilities corresponding to different signal-to-noise ratios are listed in Table 3. The average performance of each classifier is presented in Table 4.

TABLE 3. Average recognition probability under different SNR.

SNR (dB)	0	2	4	6	8	10
Average Recognition Probability (%)	83.2	85.5	90.2	89.4	93.4	94.3

TABLE 4. Comprehensive performance of the classifier.

Classifier	BP	NB	DBN	MLP	SVM
Average Recognition Probability (%)	84.0	94.1	90.8	96.4	81.0

Under the experimental conditions considered in this paper, the performance of each classifier is different. The deep learning DBN algorithm generally requires a large amount of data, which is limited by the amount of sample data trained. The performance, as described by the experimental results reported in this paper, is slightly lower than that for the algorithm of machine learning. In the figure, for the BP neural network and MLP, performance degradation can be noted with the increase in the SNR. The reason is likely that the input of all the nodes in the next layer of the back propagation is related to the output of each node in the previous layer, and it is iterated back and forth many times. In this experiment, the number of training instances is set as 200; however, in the process of iteration, it is easy to fall into local convexity, thereby generating the above-mentioned results. Table 3 presents the simulation result for SNR = 10 dB, which is the same condition as that introduced in [3], [7]. We observe that the proposed recognition technology achieves outstanding performance in classifying all the seven RASPs. Table 4 presents the confusion matrix for SNR = 6 dB for the proposed recognition technology in classifying the RASPs. The columns indicate the real RASPs, whereas the rows express the classification results obtained using the proposed recognition technology. The data in the table corresponds to the BP neural network, SVM, DBN, MLP and NB from left to right. Table 5 presents the simulation result for SNR = 10 dB, and we observe that the proposed recognition technology achieves outstanding performance in classifying all the seven RASPs with an average SRP of 90%.

Table 6 shows the required computational time for the five kinds of classifiers for SNR = 6 dB. It can be seen that the CTs required for neural networks, machine learning, and deep learning vary considerably. Among these classifiers, the SVM takes the least time; however, it has a lower SRP. The DBN of the deep learning algorithm is extremely time consuming. However, relatively, the recognition rate is extremely high and stable, and the SRP is more than 90%.

The second experiment involves a comparison with the findings reported in the recent literature. The classifier methods NB, ANN and SVM are considered, and the experimental conditions all correspond to the same environment. Fig. 12 shows the results of a comparative experiment with literature [3], which indicate the superiority of the proposed algorithm and its robustness to noise.
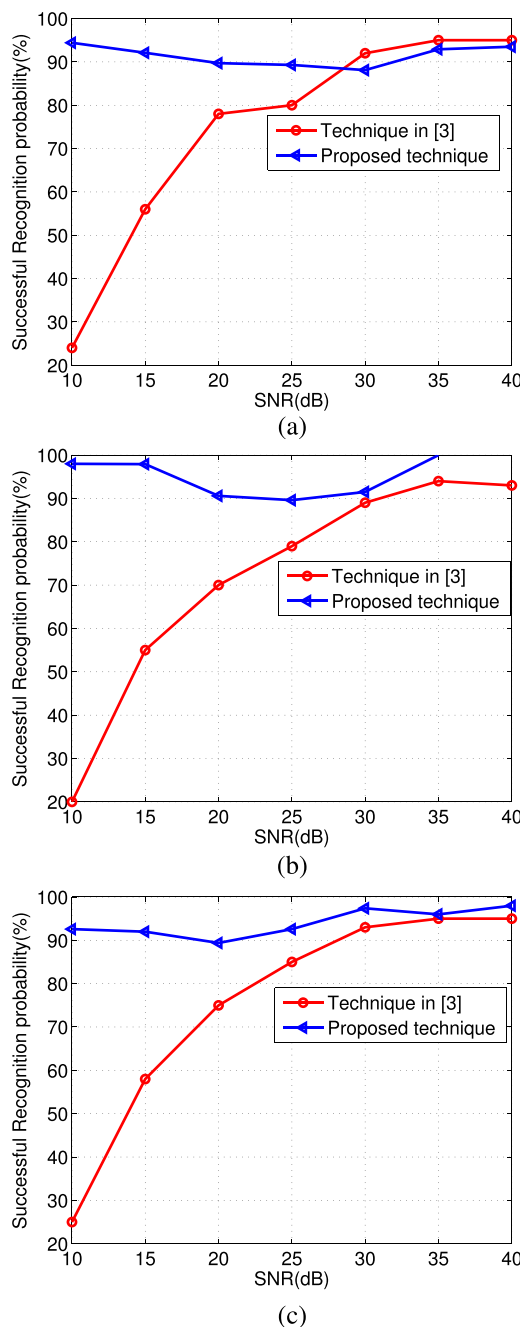

FIGURE 12. Comparison of simulation performance with literature [3]. (a) NB (b) ANN (c) SVM.

Fig. 13 shows the comparison with the technique reported in literature [7]; the experimental environment is the same, and only the average performance of all the classifiers is determined. The result of the proposed method is compared to the result obtained in [7], and the proposed technique exhibits considerable improvement, overall.

This significant improvement can be attributed to the fact that the proposed method utilizes the visibility input that has complex network information, and the input feature and the set of the five classifier parameters are designed to maximize the classification performance.

TABLE 5. Confusion matrix for the proposed approach at SNR of 6dB.

RASP	CS	SS	COS	HS	RS	PAS	PAAS
CS	86/89/92/95/94	12/9/5/4/4	8/7/4/2/0	4/2/1/4/0	2/0/0/1/2	0/0/0/0/0	0/0/0/0/0
SS	12/7/6/3/5	82/85/94/90/91	6/5/2/3/2	7/5/3/2/1	5/0/0/0/1	0/0/0/0/0	0/0/0/0/0
COS	2/4/2/2/1	6/6/1/6/4	84/83/94/91/96	7/6/6/2/3	2/5/0/0/3	0/0/0/0/0	0/0/0/0/0
HS	0/0/0/0/0	0/0/0/0/0	2/5/0/4/2	82/87/90/92/96	3/1/1/3/2	0/5/1/3/3	0/3/1/4/4
RS	0/0/0/0/0	0/0/0/0/0	0/0/0/0/0	0/0/0/0/0	88/94/99/96/92	0/5/1/3/3	0/3/1/4/4
PAS	0/0/0/0/0	0/0/0/0/0	0/0/0/0/0	0/0/0/0/0	0/0/0/0/0	87/84/91/90/94	14/17/8/4/3
PAAS	0/0/0/0/0	0/0/0/0/0	0/0/0/0/0	0/0/0/0/0	0/0/0/0/0	13/11/8/7/3	86/80/91/92/93

TABLE 6. Computational time for the proposed approach at SNR of 6dB.

Clssifier	BP	SVM	DBN	MLP	NB
CT	246.065s	30.302s	10986.809s	736.751s	432.274s

The overall results show significant improvements compared with those for the two RASP recognition methods. When the NB algorithm is applied in the case of SNR>30 dB, the SRP of the proposed recognition technology is slightly lower than that reported in literature [3]; however, this technique still exhibits considerable advantages overall, especially when compared to the ANN and SVM classifiers. In the case of reference [7] , the SRP in this paper is based on the overall recognition probability. It can be seen that the proposed recognition technology also has a high SRP in the case of low SNRs, and the performance improvement is notable. As a result, the proposed recognition technology can successfully classify all the seven RASPs considered in this paper, namely, CS, SS, COS, HS, RS, PAS, and PAAS.

The research results in this paper are based on the detection of the main lobe of the radar signal. For an LPI radar with a low SNR, this paper discusses the identification of the phased array RASP. In practice, if an EW receiver can detect the exact RASP signal of the enemy, the proposed method provides a favorable basis for the radar source identification. However, the research in this paper has certain limitations. For example, the radar side has multiple radars working simultaneously, and the main lobe is not easy to detect; moreover, when the tracking radar approaches the target, the signal transmission power is reduced.

V. CONCLUSION

This paper proposes a technique to recognize the RASP by using the VG method. First, the seven RASPs are modeled. Subsequently, the time series of the RASP is converted into a visibility graph, and the VG feature extraction is performed. Finally, the extracted six types of features are sent to the classifier. The innovation of this paper lies in the first complete introduction of the model expressions for various radar scanning patterns. Furthermore, we combine these expressions with the VG method to convert the model into a complex network. Finally, we utilize the deep learning, machine learning, and neural network approaches to identify the signals. The average recognition probability is generally greater than 90% when the SNR is greater than 4 dB. The classification performance is excellent, and the simulation experiment demonstrates the effectiveness of the algorithm.

This study presents an important advancement in the domain of EW work and provides theoretical support for future ELINT workers. However, due to the limitations of the real conditions and the model capacities, several problems remain to be solved. In the future, we will study side lobe reception at a low SNR and in the presence of clutter. Moreover, studying the conformal phased array radar and multipolarized phased array radar are future research directions.

REFERENCES

[1] R. G. Wiley and I. Ebrary, *ELINT : The Interception and Analysis of Radar Signals*. Norwood, MA, USA: Artech House, 2006.

[2] D. Adamy, *Introduction to Electronic Warfare Modeling and Simulation*. Chennai, India: Scitech Publications, 2006.

[3] B. Barshan and B. Eravci, "Automatic radar antenna scan type recognition in electronic warfare," *IEEE Trans. Aerosp. Electron. Syst.*, vol. 48, no. 4, pp. 2908–2931, Oct. 2012.

[4] S. Ayazgok, C. Erdem, and M. T. Ozturk, "Automatic antenna scan type classification for next-generation electronic warfare receivers," *IET Radar, Sonar Navigat.*, pp. 466–474, 2018.

[5] Y. H. Kim, W. J. Kim, and K. H. Song, "Modeling of a radar signal for scan pattern," in *Proc. IEEE Military Commun. Conf.*, Oct. 2010, pp. 1–6.

[6] Z. Li, "Scanning beam analysis of radar reconnaissance equipment interception," (in Chinese), *Ship Electron. Countermeasure*, vol. 1, pp. 1–7, Jan. 2000.

[7] Y. H. Kim, K. H. Song, and J. W. Han, "RASP analysis for reduction of false identification in electronic warfare support systems," *IET Radar, Sonar Navigat.*, vol. 8, no. 7, pp. 719–728, 2014.

[8] X. Zhang, C. Hao, S. Zhang, and L. Zheng, "Characterization and identification of active electronically scanned array radar," in *Proc. IEEE Int. Geosci. Remote Sens. Symp. (IGARSS)*, Jul. 2017, pp. 2318–2321.

[9] R. Zhang, B. Ashuri, and Y. Deng, "A novel method for forecasting time series based on fuzzy logic and visibility graph," *Adv. Data Anal. Classification*, vol. 11, no. 4, pp. 759–783, 2017.

[10] Z. Zhang, Y. Qin, and L. Jia, "Visibility graph feature model of vibration signals: A novel bearing fault diagnosis approach," *Materials*, vol. 11, no. 11, p. 2262, 2018.

[11] J. Iacovacci and L. Lacasa, "Visibility graphs for image processing," *IEEE Trans. Pattern Anal. Mach. Intell.*, to be published.

[12] S. Chen, Y. Hu, and S. Mahadevan, "A visibility graph averaging aggregation operator," *Phys. A, Stat. Mech. Appl.*, vol. 403, pp. 1–12, 2014.

[13] P. Xu, R. Zhang, and Y. Deng, "A novel visibility graph transformation of time series into weighted networks," *Chaos, Solitons Fractals*, vol. 117, pp. 201–208, 2018.

[14] C. Dharmagunawardhana, S. Mahmoodi, and M. Bennett, "Rotation invariant texture descriptors based on Gaussian Markov random fields for classification," *Pattern Recognit. Lett.*, vol. 69, pp. 15–21, 2016.

[15] S. Salari, I.-M. Kim, S. Rajan, and F. Chan, "Blind compressive-sensing-based electronic warfare receiver," *IEEE Trans. Aerosp. Electron. Syst.*, vol. 53, no. 4, pp. 2014–2030, Aug. 2017.

[16] L. Cheng, W. Wei, and S. Longfei, "Automatic identification method of radar antenna scanning method," *J. Nat. Univ. Defense Technol.*, vol. 3, pp. 159–166, Aug. 2014.

[17] J. Liu, H. Wu, and B. Rao, *Radio-Injection Semi-Physical Simulation of Radar Electronic Warfare System*. Beijing, China: Aerospace Publishing House, 2016, pp. 145–149.

[18] B. R. Mahafza, *Matlab Simulations for Radar Systems Design*. Boca Raton, FL, USA: CRC Press, 2003.

[19] N. Dame, "Statistical mechanics of complex networks," *Rev. Modern Phys.*, vol. 74, no. 1, p. 12, 2002.

[20] R. Diestel, "Graph-theory," *Math. Gazette*, vol. 173, no. 502, pp. 67–128, 2000.

[21] M. E. Newman, "Scientific collaboration networks. I. Network construction and fundamental results," *Phys. Rev. E, Stat. Phys. Plasmas Fluids Relat. Interdiscip. Top.*, vol. 64, 2001, Art. no. 016131.

[22] M. E. J. Newman, "Assortative mixing in networks," *Phys. Rev. Lett.*, vol. 89, no. 20, pp. 208–701, 2002.

[23] T. M. Cover and J. A. Thomas, *Elements of Information Theory*. 2003.

[24] J. Kim and T. Wilhelm, "What is a complex graph?" *Phys. A, Stat. Mech. Appl.*, vol. 387, no. 11, pp. 2637–2652, 2008.

[25] M. Ahmadlou, H. Adeli, and A. Adeli, "New diagnostic EEG markers of the Alzheimer's disease using visibility graph," *J. Neural Transmiss.*, vol. 117, no. 9, pp. 1099–1109, 2010.

[26] S. Haykin, *Neural Networks: A Comprehensive Foundation*, 2nd ed. Upper Saddle River, NJ, USA: Prentice-Hall, 1994, pp. 1–256.

[27] S. Theodoridis, "Pattern recognition," *Encyclopedia Inf. Syst.*, vol. 21, no. 16, pp. 459–479, 2003.

[28] K. P. Murphy, "Machine learning : A probabilistic perspective," *Chance*, vol. 27, no. 2, pp. 62–63, 2012.

[29] I. Goodfellow, Y. Bengio, and A. Courville, *Deep Learning*, vol. 1. Cambridge, MA, USA: MIT Press, 2016.

[30] Y. LeCun, Y. Bengio, and G. Hinton, "Deep learning," *Nature*, vol. 521, no. 7553, p. 436, 2015.

[31] R. M. Neal, "Connectionist learning of belief networks," *Artif. Intell.*, vol. 56, no. 1, pp. 71–113, 1992.

[32] T. W. Jeffrey, *Phased-Array Radar Design: Application of Radar Fundamentals*. Edison, NJ, USA: IET, 2009.

[33] P. Eskelinen, "Detecting and classifying low probability of intercept radar," *IEEE Aerosp. Electron. Syst. Mag.*, vol. 19, no. 5, pp. 42–44, May 2004.

[34] A. Ghasempour and S. K. Jayaweera, "Data synchronization for throughput maximization in distributed transmit beamforming," in *Proc. Cognit. Commun. Aerosp. Appl. Workshop (CCAA)*, Cleveland, OH, USA, 2017, pp. 1–4.

XINYING FU received the bachelor's degree from Harbin Engineering University, in 2017. She is currently pursuing the master's degree in information and communication engineering with the School of Information and Communication Engineering, University of Electronic Science and Technology of China. Her main research direction is radar signal processing.
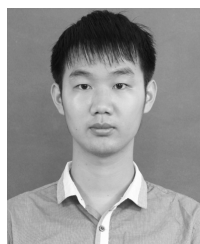
KAILI JIANG received the B.S. degree from the University of Electronic Science and Technology of China, Chengdu, China, in 2013, where she is currently pursuing the Ph.D. degree with the School of Information and Communication Engineering. Her research interests include wideband spectrum sensing, sparse/compressive sensing, and radar signal processing.

YUAN ZHAO received the bachelor's degree from the University of Electronic Science and Technology of China, in 2013, and the Ph.D. degree from the University of Electronic Science and Technology of China, in 2019. His current research direction is mainly electronic support.

TAO WAN received the B.S. degree from the Harbin University of Commerce, Harbin, China, in 2017. He is currently pursuing the Ph.D. degree with the University of Electronic Science and Technology of China (UESTC). He is interested in electronic reconnaissance and is mainly engaged in electronic countermeasures, signal processing, and machine learning.

BIN TANG is currently a Professor with the University of Electronic Science and Technology of China. His research interests include complex/complex modulation LPI and new system radar reconnaissance and interference technology, adaptive radar reconnaissance and interference technology, networked radar countermeasure technology, and broadband/ultrawideband radar digital reconnaissance receiving and interference technology.

• • •